Tellus (1996), 48A, 122–137
Printed in Belgium – all rights reserved

TELLUS
ISSN 0280–6495

Energy and enstrophy conservation properties of high-order non-oscillatory advection schemes

By ELÍAS VALUR HÓLM, *Department of Meteorology, Arrhenius Laboratory, Stockholm University, S-106 91 Stockholm, Sweden*

(Manuscript received 6 September 1994; in final form 17 February 1995)

ABSTRACT

The dissipative behaviour as well as the conservative and spectral properties of a class of high-order non-oscillatory advection schemes, developed by Hólm (1995), are investigated for the incompressible, two-dimensional, constant density Euler equations. These equations are closely connected to large scale atmospheric flows. The advection schemes are applied to two different forms of the governing equations: the vorticity-stream function form and the momentum-pressure form. For both forms, the advection schemes are found to be essentially kinetic energy conserving. This includes several tests, for example isotropic turbulence simulations. Furthermore, enstrophy is dissipated at a correct rate predicted by theory. In turbulence simulations, enstrophy spectra with an inertial subrange slope of ~ -1.2 are observed, in accordance with theory. The time-evolution of the kinetic energy, enstrophy and the enstrophy dissipation are also found to be consistent with the theory of viscous, incompressible, two-dimensional turbulence. For the shorter waves, the spectral amplitudes fall off more rapidly than what is expected for the real flow. It is shown that this damping of the short waves is necessary for obtaining non-oscillatory physical fields, since otherwise oscillations would appear due to Gibbs' phenomenon. Thus it is impossible to have a perfect spectrum and a non-oscillatory physical field at the same time, and a compromise between these two aspects needs to be found. If it is desirable that the physical field be non-oscillatory, then the high-order, non-oscillatory schemes give better conservation properties and a more realistic spectrum than a reference energy and enstrophy conserving scheme supplied with artificial viscosity. In general, it is found that high-order, non-oscillatory advection schemes have the properties required for accurate simulations of large-scale atmospheric motions.

1. Introduction

In all atmospheric models a balance has to be found between, on the one hand, an accurate description of the physical phenomena of interest and, on the other hand, the model resolution, so that the simulation can be performed within realistic time limits set by the available computer facilities. In this context, high-order non-oscillatory advection schemes are of interest, since they deliver accurate simulations at low model resolutions (Bell et al., 1989; E and Shu, 1994; Hólm, 1995) and automatically ensure that the simulations are nonlinearly stable and without unphysical oscillations (see, e.g., Hirsch (1990) for a review). In the present paper the properties of the high-order, non-oscillatory advection schemes of Hólm (1995) are investigated, with the main focus upon the conservative and spectral behaviour of the schemes in two-dimensional incompressible flows. This system contains the basic features of large scale atmospheric and oceanographic flows (Monin and Ozmidov, 1985). Measurements of atmospheric wind and temperature wavenumber spectra (Gage and Nastrom, 1986) show this similarity on scales above 700 km. For the present study, two different formulations of the governing equations are used. In the first formulation, the vorticity (a scalar) is advected, with the velocity field determined from a stream function. In the second formulation, the momentum (a vector) is advected, with the pressure gradient appearing as a source term (which makes it necessary to address the accurate inclusion of source terms in the time integration as well). Both formulations have important correspondences in elastic flows: the momentum-mass form and the vorticity-divergence form.

A knowledge of the conservative and the spectral properties of an advection scheme is important for assessing the realism of the simulations performed with the scheme, and for a comparison with simulations performed with other advection methods. In a perfect model the spectrum of the variables of interest should be indistinguishable from the spectrum of the natural phenomena in the resolvable wavenumber range (Gage and Nastrom, 1986, for a comprehensive evaluation of measured atmospheric spectra). Further the basic physical conservation laws of the system should remain fulfilled for the "truncated" model, which simply means that model variables representing a given volume should equal the average value of the real atmosphere inside this volume. From the theory of incompressible two-dimensional turbulence (Monin and Ozmidov, 1985) it is also known that the kinetic energy cascades towards larger scales, which are essentially unaffected by weak dissipation, and that the enstrophy cascades towards smaller scales, which are affected by dissipation. Thus kinetic energy should be essentially conserved, while enstrophy should be dissipated in simulations of large scale atmospheric flows. In between the large scale and the dissipative scale the enstrophy flows at a constant rate, unaffected by the dissipation. As a consequence the spectrum contains a range with constant spectral density slope, the inertial subrange. The slope of the inertial subrange has been theoretically estimated as $k^{-3} - k^{-4}$ (Lesieur, 1990), and measured as k^{-3} in the atmosphere (Gage and Nastrom, 1986).

A strong motivation for using high-order non-oscillatory advection schemes is the nonlinear stability and suppression of unphysical oscillations inherent in these methods. With traditional centred-in-space finite difference schemes and spectral schemes it is necessary to introduce artificial viscosity terms in the model equations to achieve nonlinear stability. But the artificial viscosity must be carefully formulated in order for the kinetic energy spectrum to become realistic (Basdevant et al., 1978). Further, as found in the review of Smagorinsky (1993), the formulation of the artificial viscosity terms and the coefficient values involved need to be adjusted for each new application. Numerical integration techniques which achieve nonlinear stability without having to use artificial viscosity have been developed by, e.g., Arakawa (1966), Arakawa and Hsu (1990), and Walsteijn (1994), based on conservation principles (e.g., energy conservation). Although the numerical instability can be eliminated with such techniques, considerable noise is often created on the smallest scales, which can interact with other variables and physical processes of the model and lead to destabilisation. Artificial viscosity (or filtering) is again needed to remove this noise (see also Walsteijn, 1994). But when an advection scheme which conserves energy and/or enstrophy, e.g., Arakawa (1966), is combined with an explicit artificial viscosity, then energy and/or enstrophy are not necessarily conserved any more. However, energy conserving and enstrophy dissipating artificial viscosity has been developed by, e.g., Sadourny and Basdevant (1985).

A characteristic of non-oscillatory advection schemes is that they have a built-in implicit diffusion, which depends on the local flow. This diffusion has several consequences for simulations using these types of advection schemes. Even if the model equations consist of the incompressible, constant density, Euler equations, which in theory have no viscosity, the result in effect agrees with the incompressible Navier-Stokes equations. Note however that near boundaries, where the friction plays a large role, the Euler equations will not agree with the Navier-Stokes equations. The theory of two-dimensional viscous turbulence can be used to predict the behaviour of certain integrals of the motion, e.g., the kinetic energy, the enstrophy and their dissipation rates. Since analytical solutions to the equations are rare, and are generally only available for very simple flows, the theory of viscous turbulence is useful for testing how the physical advection process is influenced by the numerical advection schemes. Further, the mathematical relations for energy and enstrophy dissipation of viscous turbulence can be used for directly estimating the magnitude of the implicit numerical diffusion present in the non-oscillatory schemes (for another approach to estimating the implicit viscosity, using numerical solutions for the laminar spread of mixing layers, see Grinstein and Guirguis, 1992).

From the above discussions, some conclusions can be drawn as to what could be required of an advection algorithm for use in large scale atmospheric flows. It is desirable to have an advection scheme which is nonlinearly stable, approximately conserves kinetic energy, dissipates enstrophy, has realistic spectra (including inertial subrange with a correct slope) and is free of unphysical oscillations. Further, when subgrid scale parametrizations are considered, one has to be certain that the magnitude of the implicit diffusion does not overshadow these processes (as when the traditional upstream scheme is used, which is certainly non-oscillatory, but also excessively diffusive). In the following sections I will investigate to what degree the schemes of Hólm (1995) can meet these requirements, but the results should be relevant for other high-order non-oscillatory advection schemes as well. For reference, the energy and enstrophy conserving scheme of Arakawa (1966) with or without (linear fourth order) artificial viscosity will be used.

The paper is organized as follows. In Section 2, some results from the theory of incompressible two-dimensional viscous turbulence are summarized. Section 3 describes the model and the numerical integration techniques. Then the accuracy and the dissipative properties of the non-oscillatory scheme is investigated in Section 4. In Section 5, turbulence simulations are used to demonstrate the main differences between the non-oscillatory scheme and the reference energy and enstrophy conserving scheme, in both physical and spectral space, and the results are compared with theory. The effect of the implicit diffusion of the non-oscillatory scheme on the spectrum are also analysed in Section 5, before the conclusions are given in Section 6.

2. Results from the theory of incompressible, viscous turbulence

The incompressible Navier-Stokes equations together with the continuity equation, which describe two-dimensional incompressible turbulence, are given by

$$u_t + (uu)_x + (vu)_y = -p_x/\rho + \nu\,\nabla^2 u, \tag{1}$$

$$v_t + (uv)_x + (vv)_y = -p_y/\rho + \nu\,\nabla^2 v, \tag{2}$$

$$u_x + v_y = 0, \tag{3}$$

where $\boldsymbol{v} = (u, v)$ is the velocity, p is pressure, ρ is the constant density and ν is the kinematic viscosity (which for atmospheric motions would be replaced by a turbulent viscosity). It is convenient to eliminate the pressure by introducing the stream function, Ψ, and the vorticity component perpendicular to the flow plane, ζ, as independent variables,

$$\boldsymbol{k} \times \nabla\Psi = -\Psi_y \boldsymbol{i} + \Psi_x \boldsymbol{j} = \boldsymbol{v}, \tag{4}$$

$$\zeta = (\nabla \times \boldsymbol{v}) \cdot \boldsymbol{k} = v_x - u_y, \tag{5}$$

where $\boldsymbol{i}$, $\boldsymbol{j}$ and $\boldsymbol{k}$ are orthogonal unit vectors. The equations for the vorticity and the stream function are given by

$$\zeta_t + (u\zeta)_x + (v\zeta)_y = \nu\,\nabla^2\zeta, \tag{6}$$

$$\nabla^2\Psi = \zeta. \tag{7}$$

In incompressible, two-dimensional turbulent flows without viscosity, momentum, vorticity, kinetic energy and enstrophy are conserved. For viscous turbulence, momentum and vorticity are still conserved, and the effect of the viscosity is to redistribute the vorticity and the momentum. But the total kinetic energy and enstrophy, E and Ω, are dissipated (Herring et al., 1974, and Monin and Ozmidov, 1985) according to

$$\begin{aligned}\frac{\mathrm{d}E}{\mathrm{d}t} &= \frac{\mathrm{d}}{\mathrm{d}t}\langle(\boldsymbol{v}\cdot\boldsymbol{v})/2\rangle \\ &= \frac{\mathrm{d}}{\mathrm{d}t}\langle(u^2+v^2)/2\rangle = -2\nu\Omega,\end{aligned} \tag{8}$$

$$\begin{aligned}\frac{\mathrm{d}\Omega}{\mathrm{d}t} &= \frac{\mathrm{d}}{\mathrm{d}t}\langle[(\nabla\times\boldsymbol{v})\cdot\boldsymbol{k}]^2/2\rangle \\ &= \frac{\mathrm{d}}{\mathrm{d}t}\langle\zeta^2/2\rangle = -2\nu P,\end{aligned} \tag{9}$$

where the total palinstrophy P has been introduced (Lesieur, 1990 and Pouquet et al., 1975)

$$\begin{aligned}P &= \langle[\nabla\times(\nabla\times\boldsymbol{v})\cdot\boldsymbol{k}]^2/2\rangle \\ &= \langle[(\zeta_x)^2+(\zeta_y)^2]/2\rangle.\end{aligned} \tag{10}$$

Here the brackets $\langle\ \rangle$ denote integration over the space domain. The kinetic energy dissipation rate is thus proportional to the enstrophy, while the enstrophy dissipation rate is proportional to the palinstrophy. In freely decaying, viscous, two-dimensional turbulence, the kinetic energy and enstrophy decrease with time. But for small viscosity, calculations show (Lesieur, 1990) that the palinstrophy increases with time to a maximum, whereafter it decreases due to the action of viscosity. As a consequence, enstrophy can be dissipated quickly without any significant decrease in kinetic energy. The dissipation of enstrophy and essential kinetic energy conservation are also characteristic of large scale atmospheric flows, and can be deduced from measured atmospheric spectra (Gage and Nastrom, 1986) as discussed in the introduction. Generally, the relation between the dissipation of kinetic energy and enstrophy depends both on the viscosity and on the initial relative magnitudes of the kinetic energy, enstrophy and palinstrophy.

Given the relations between the dissipation of kinetic energy and enstrophy, eqs. (8–10), it is possible to estimate the effective viscosity implicit in a given advection scheme from, for example, eq. (9)

$$\nu_e = -\frac{1}{2P}\frac{d\Omega}{dt}. \tag{11}$$

The enstrophy dissipation, rather than the kinetic energy dissipation, is preferred for the determination of the viscosity, since the kinetic energy dissipation has a much smaller magnitude for a small viscosity. The effective viscosity can be used, instead of the explicit viscosity appearing in the equations with viscosity, to calculate the characteristic parameters of the flow. As in Herring et al. (1974), it is possible to characterize the size of the eddies contributing most to the enstrophy (the integral-scale L) and to the enstrophy dissipation (the scale l). For each of these length scales, Reynolds numbers can also be defined if the effective viscosity in eq. (11) is used,

$$L = k_L^{-1} = \frac{E^{1/2}}{(2\nu_e P)^{1/3}}, \tag{12}$$

$$R_L = \frac{E^{1/2}L}{\nu_e} = \frac{E}{(2\nu_e^4 P)^{1/3}}, \tag{13}$$

$$l = \left(\frac{\Omega}{2P}\right)^{1/2}, \tag{14}$$

$$R_l = \frac{(l\Omega^{1/2})\, l}{\nu_e} = \frac{\Omega^{3/2}}{2\nu_e P}. \tag{15}$$

Further, an enstrophy dissipation wavenumber is defined by

$$k_d = (2P/\nu_e^2)^{1/6}. \tag{16}$$

Motions on scales larger than this wavenumber are not influenced significantly by scales much smaller than this wavenumber, and a two-dimensional turbulence simulation truncated at or above k_d can be considered as a closed system. If there is a separation in the integral-scale and the dissipative-scale wavenumbers, such that $k_L \ll k \ll k_d$, then it is possible to simulate an inertial subrange, provided that the simulation is accurate for these wavenumbers. The length scales L and l can also be inferred from the spectrum of the motion: L corresponds to the maximum in the enstrophy and l corresponds to the maximum in the palinstrophy. If these two maxima are well separated, and the flow is accurately simulated for scales larger than l, then the possibility of simulating an inertial subrange follows. The energy spectrum should have a slope between -3 and -4 in the inertial subrange (Brachet et al., 1988; Lesieur, 1990), corresponding to a -1 to -2 enstrophy slope.

3. Numerical integration techniques

In the simulations, both the momentum-pressure form in eqs. (1–3) and the vorticity-stream function form in eqs. (4–7) are used, but without explicit viscosity (i.e., $\nu = 0$). The high-order non-oscillatory advection schemes with forward-in-time differencing described in Hólm (1995) are used for advecting the velocity and vorticity, and a standard second order successive-over-relaxation scheme is used to solve the equations for pressure and for the stream function. For the evaluation of pressure derivatives, the fourth order accurate formulas of Gupta (1991) are used. This helps to prevent re-introduction of over/undershooting caused by the solution of the elliptic equation, as shown in Hólm (1995). Three versions of the non-oscillatory scheme are used, which use second, fourth or sixth degree polynomials to represent the advected variable within the grid-cells. These schemes are referred to as FPM2, FPM4 and FPM6. Furthermore, FPM2/M and FPM2/V etc. will be used to separate simulations performed with the momentum-pressure (M) and the vorticity-stream function (V) form. The time-accuracy of the complete algorithm is second order. The momentum-pressure form of the algorithm advances the solution from timelevel n to $n+1$ with a timestep Δt, employing the fully second order time-accurate correction of the forward-in-time algorithm given by Smolarkiewicz and Margolin (1993),

$$\boldsymbol{v}^{n+1/2} = 1.5\boldsymbol{v}^n - 0.5\boldsymbol{v}^{n-1}, \tag{17a}$$

$$\boldsymbol{v}^{\mathrm{ad}} = A\left(\boldsymbol{v}^n - \frac{\Delta t}{2\rho}\nabla p^n, \boldsymbol{v}^{n+1/2}, \Delta t\right), \tag{17b}$$

$$\nabla^2 p^{n+1} = \frac{2\rho}{\Delta t}\nabla\cdot\boldsymbol{v}^{\mathrm{ad}}, \tag{17c}$$

$$\boldsymbol{v}^{n+1} = \boldsymbol{v}^{\mathrm{ad}} - \frac{\Delta t}{2\rho}\nabla p^{n+1} \tag{17d}$$

The vorticity-stream function form of the equations is advanced with the following second order algorithm,

$$\zeta^{n+1/2} = A(\zeta^n, \boldsymbol{v}^{n-1/2}, \Delta t/2), \tag{18a}$$

$$\nabla^2\Psi^{n+1/2} = \zeta^{n+1/2}, \tag{18b}$$

$$\zeta^{n+1} = A(\zeta^n, \boldsymbol{v}^{n+1/2}, \Delta t). \tag{18c}$$

In the above equations, the operator A denotes the advection scheme, so that in, e.g., eq. (18c), an advection step with length Δt is performed with the fluxes calculated from ζ^n and advective velocity $\boldsymbol{v}^{n+1/2}$. Note that in eq. (18a), $\boldsymbol{v}^{n-1/2}$ is used, since it is already available and enough for an overall second order accuracy (Bell et al., 1989). But it would also be possible to use $\boldsymbol{v}^{n+1/4}$, which can be obtained from linear extrapolation. In the first timestep, only initial values are available, so a simple forward step is employed.

For reference, the second order energy and enstrophy conserving advection scheme of Arakawa (1966) is used together with a fourth order linear diffusion, $\kappa\nabla^4\zeta$ (with a standard second order discretization of the biharmonic operator). For the comparison with the non-oscillatory schemes, the magnitude of the diffusion coefficient is tuned for each case to be the minimum necessary for avoiding visible unphysical oscillations. For the time-stepping, eqs. (18a–c) are used, except that ζ^n is replaced by $\zeta^{n+1/2}$ in eq. (18c). This scheme is refereed to as AEE, and AEE + DF if diffusion is included.

4. Accuracy and dissipative properties

In Hólm (1995), a first-order accurate forward-in-time integration of the momentum-pressure form is found to be kinetic energy dissipating. The largest source of this dissipation lies in the source term integration (the pressure gradients). By using fully second order accurate modification of the forward-in-time integration with source terms (Smolarkiewicz and Margolin, 1993) the largest source of dissipation is removed, and the resulting kinetic energy conservation is better than for reference simulations from the literature (Bell et al., 1989). In this section, the accuracy and dissipative properties of the momentum-pressure form, eqs. (1–3), will be compared with the vorticity-stream function form, eqs. (4–7), which has no source terms. The accuracy and the effective viscosity of the two formulations can be assessed by a comparison with an analytic solution. For this purpose a steady state solution of the inviscid equations is used as an initial condition.

The steady state solution (initial condition), together with the corresponding viscous solution is given in terms of the vorticity (Taylor, 1960)

$$\zeta(x, y, 0) = 2a\sin ax\sin ay, \tag{19a}$$

$$\zeta(x, y, t) = 2a\sin ax\sin ay\exp(-2a^2\nu t). \tag{19b}$$

This solution consists of an infinite system of vortices rotating in alternate directions (see Fig. 1 of Taylor (1960)). To demonstrate the main characteristics of the integration algorithms, a long wave with wavenumber $a = 1$ and a short wave with $a = 4$ are used. The test domain is a doubly periodic square with dimension $L = 2\pi$ and gridsize $\Delta x = \Delta y = 2\pi/N$. In the tests the initial condition is translated half a gridlength in each direction, $\zeta^0_{j,k} = 2a\sin a(j\,\Delta x - \Delta x/2)\sin a(k\,\Delta y - \Delta y/2)$. The equations are integrated to $t = 10$ time-units, with a constant maximum Courant–Friedrichs–Lewy number, $\mathrm{CFL}_{\max} = \max(|u|\,\Delta t/\Delta x, |v|\,\Delta t/\Delta y) = 0.5$, and at 64^2 resolution.

In Table 1, the dissipative properties of the non-oscillatory schemes and the reference scheme (Arakawa, 1966) are summarized. For the long wave solution, both kinetic energy and enstrophy are conserved better than ca. 99.8% for all second order accurate versions of the non-oscillatory scheme. If FPM2 is applied to the momentum-pressure form with a first order time-stepping, then

Table 1. *Dissipative properties of the non-oscillatory and the reference advection schemes for the analytic tests* ($CFL_{max} = 0.5$, 64^2 *resolution*, $t = 10$)

	Long-wave test ($a = 1$)*			Short-wave test ($a = 4$)*		
Scheme**	E_{10}/E_0	Ω_{10}/Ω_0	ν_e, eq. (11)	E_{10}/E_0	Ω_{10}/Ω_0	ν_e, eq. (11)
US	0.597	0.618	1.2×10^{-2}	0.026	0.029	2.9×10^{-3}
FPM2/O(Δt)	0.801	0.804	5.4×10^{-3}	0.124	0.128	2.4×10^{-3}
FPM2/M	0.99781	0.99782	5.5×10^{-5}	0.626	0.630	7.6×10^{-4}
FPM4/M	0.99872	0.99874	3.2×10^{-5}	0.745	0.754	4.5×10^{-4}
FPM6/M	0.99872	0.99874	3.1×10^{-5}	0.746	0.758	4.4×10^{-4}
FPM2/V	0.99948	0.99949	1.3×10^{-5}	0.913	0.909	1.3×10^{-5}
FPM4/V	0.99997	0.99998	4.5×10^{-7}	0.976	0.971	1.3×10^{-5}
FPM6/V	0.99998	0.99999	2.8×10^{-7}	0.983	0.970	1.3×10^{-5}
AEE	1.00000	1.00000	0	1.00000	1.00000	0
AEE + DF	0.99745	0.99745	6.4×10^{-5}	0.528	0.528	1.0×10^{-3}

* Initial energy, enstrophy and palinstrophy are: for $a = 1$, $E_0 = 0.25$, $\Omega_0 = 0.5$, $P_0 = 1.0$; for $a = 4$, $E_0 = 0.25$, $\Omega_0 = 8.0$, $P_0 = 243$.

** US = upstream scheme, O(Δt). FPM2/O(Δt) = momentum-pressure form, O(Δt). FPM2, 4, 6/M = momentum-pressure form, O(Δt^2). FPM2, 4, 6/V = vorticity-stream function form, O(Δt^2). AEE = Arakawa (1966) energy and enstrophy conserving scheme applied to the vorticity-stream function form, O(Δt^2). AEE + DF = AEE with linear artificial viscosity, $3.2 \times 10^{-5}\, \nabla^4 \zeta$, O($\Delta t^2$).

the conservation drops to 80% (cf. 60% for the upstream scheme). Thus a second order time-accuracy is essential for conservation. In the short wave test, the dissipation is larger. This can be understood by considering the relation of the initial energy, enstrophy and palinstrophy of the two tests. The ratio of initial enstrophy to kinetic energy is 2 for the long wave test and 36 for the short wave test. From the energy and enstrophy dissipation relations, eqs. (8–9), it is seen that this causes a more rapid dissipation for the short wave. These deviations from the stationary analytical solutions are unavoidable when non-oscillatory schemes are used, due to the built-in diffusion. If the Arakawa energy and enstrophy conserving scheme is used, then there is an exact conservation of the initial condition. The reason for the excellent behaviour of the Arakawa scheme is that the discrete Jacobian used for evaluating the advection is exactly zero for the analytical initial condition. However, in atmospheric flows, the Arakawa scheme has to be supplemented with an explicit artificial viscosity to hinder the occurrence of small scale oscillations. When the Arakawa scheme is used together with a linear fourth order diffusion ($\kappa = 3.2 \times 10^{-5}$ m^2/s, which at 64^2 resolution corresponds to the minimum viscosity needed for removing the oscillations in the simulations of Subsection 5.1), then the dissipation is somewhat larger than for the least accurate high-order non-oscillatory scheme, FPM2/M (see Table 1 for notation). The effective viscosity of the different schemes are also given in Table 1. The non-oscillatory schemes have larger dissipation when applied to the momentum-pressure form than when applied to the vorticity-stream function form. The vorticity-stream function form versions FPM4/V and FPM6/V have two orders of magnitude less effective viscosity than the other schemes for the long wave tests, including the Arakawa scheme with artificial diffusion. This is an advantage for example when atmospheric boundary layer processes are parameterized in a model which uses either one of these two advection schemes. Then the small numerical viscosity of the non-oscillatory schemes is likely to be negligible as compared to the effect of physical processes.

In Fig. 1, the errors of the different second-order accurate schemes are compared. The L_2-norm is used for calculating the error of the x-component of the velocity and of the vorticity: $\|u\|_2 = [\sum (u^{\mathrm{n}} - u^{\mathrm{a}})^2/N]^{1/2}$, where u^{n} is the numerical solution, u^{a} is the analytical solution, and the summation is performed over all N gridpoints of the model (similar for the vorticity ζ). The first thing which strikes the eye is that for the vorticity-

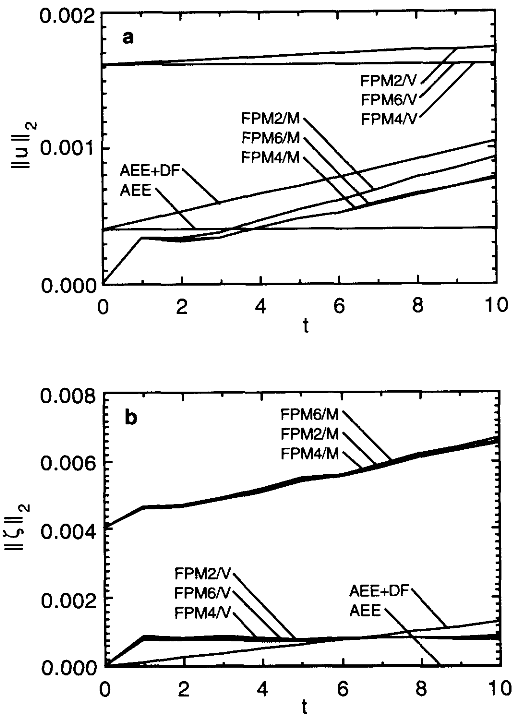

Fig. 1. L_2-errors for the analytic long wave test for the non-oscillatory schemes and the reference scheme for $t = 0$–10 ($a = 1$, 64^2 resolution, $\mathrm{CFL}_{\max} = 0.5$, ca. 200 timesteps). The notations for the different schemes are the same as in Table 1. (a) Velocity error $\|u\|_2$. (b) Vorticity error $\|\zeta\|_2$.

stream function formulation $\|u\|_2$ is nonzero at $t = 0$, Fig. 1a, and for the momentum-pressure formulation $\|\zeta\|_2$ is nonzero at $t = 0$, Fig. 1b. The reason is that these quantities are diagnosed. The nonzero error at $t = 0$ is the truncation error of the diagnostic formulas, which should be subtracted from the total error in order to obtain the error caused by the model integration. Since the momentum will normally be needed as an output, the accuracy, of e.g., the Arakawa scheme becomes comparable to the other schemes when the momentum field is diagnosed, in spite of its extremely accurate vorticity field. In Fig. 1a, it can be seen that FPM2 is less accurate than FPM4 and FPM6, which are comparable in accuracy. Actually, FPM4 is slightly more accurate, which can be related to that the possible increase in accuracy with FPM6 is much less than the second order truncation error of the total integration algorithm. Instead of increasing the accuracy, the small modifications then affect the remainder of the algorithm unfavourably. The advantage of FPM6 is noticed in flows involving sharp gradients, where FPM6 can, e.g., resolve thinner shear layers than FPM4. At last, it is noticeable that the error increases nearly linearly with time for the non-oscillatory schemes, which is consistent with the presence of implicit viscosity. In this case the implicit viscosity is a disadvantage, but in real atmospheric flows, which are always at least weakly dissipative, it could be that the presence of implicit viscosity does not affect the simulation negatively (this question will be investigated further in the following section).

In conclusion, the dissipation of kinetic energy and enstrophy is small for both the momentum-pressure and the vorticity-stream function versions of the high-order non-oscillatory advection schemes. FPM4 applied to the vorticity-stream function form is the best option of the tested versions (FPM6 gives comparable results, but at higher computational costs): kinetic energy and enstrophy are conserved better than 99.99% for long waves, and the effective viscosity is two orders of magnitude less than with the other tested schemes.

5. Turbulence simulations

In this section, further tests with time-dependent turbulent flows are performed. No analytic solutions are available, but a look at the solution in physical space immediately reveals if there are artificial oscillations present, and a look at the enstrophy and palinstrophy spectra reveal whether the simulations are consistent with the theory of two-dimensional, incompressible, viscous turbulence. In particular, the slope of the spectrum in the inertial subrange (when it is possible to simulate) and time-development of the kinetic energy, enstrophy and palinstrophy can be compared with the theoretical predictions (Lesieur, 1990). The spectrum also reveals how the implicit viscosity of the non-oscillatory scheme affects different scales of the motion.

5.1. A comparison of the physical and spectral solutions

High-order, non-oscillatory advection schemes give very "pleasant looking" solutions in physical space, and resemble what is expected from the atmosphere. But how do these solutions look in spectral space? A shear layer simulation given by Bell et al. (1989) is used for investigating the spectral appearance of a simulation which is smooth in physical space. This test was also used by Hólm (1995) for the momentum-pressure form of the equations. Since the initial shear layer quickly develops sharpened gradients which become unresolvable on the grid, the kinetic energy will

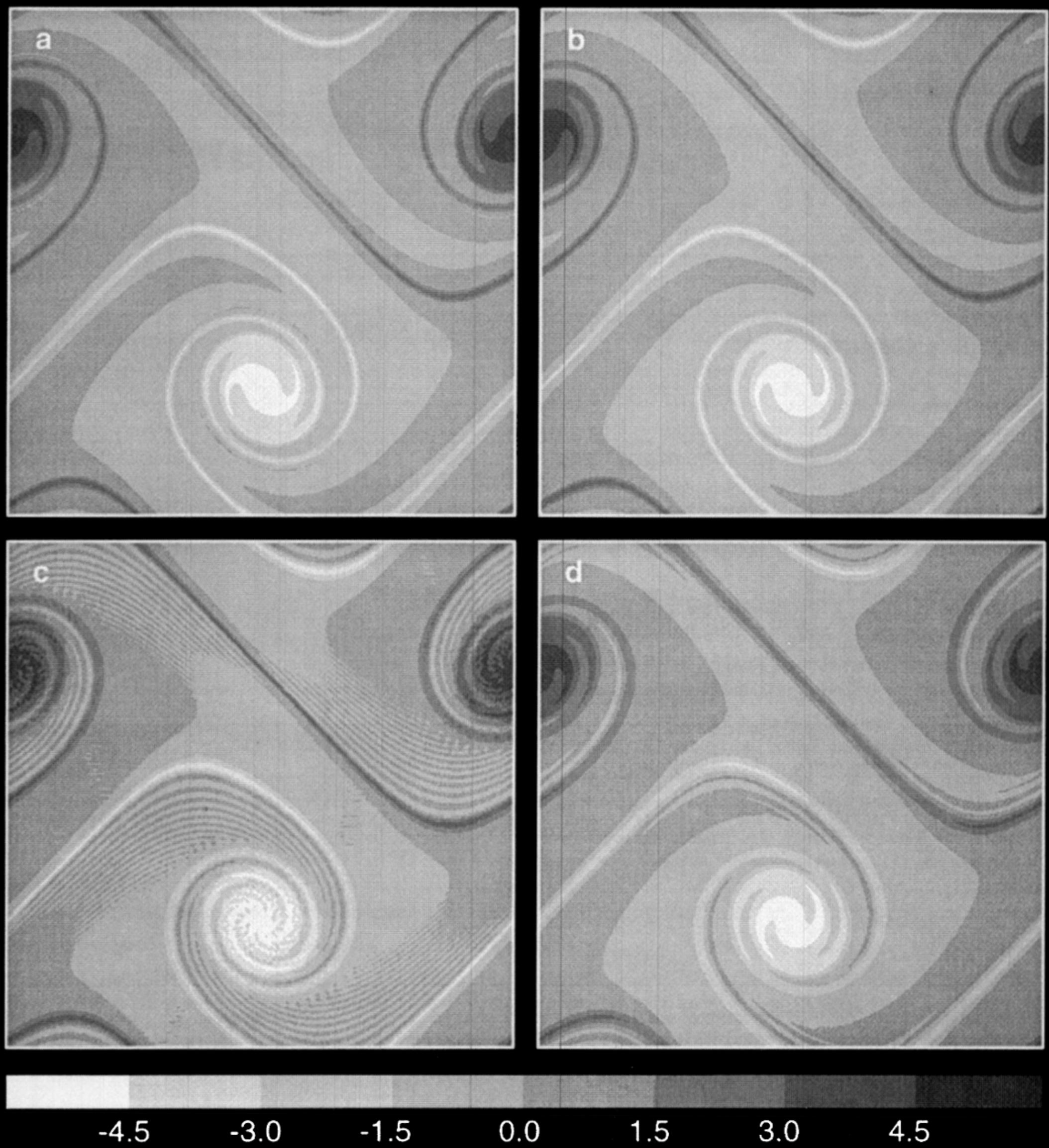

Fig. 2. Vorticity field for the shear layer simulation at the time of maximum enstrophy dissipation, $t = 8$ (256^2 resolution, $CFL_{max} = 0.5$). (a) FPM4 applied on the momentum-pressure form. (b) FPM4 applied on the vorticity-stream function form. (c) Arakawa energy and enstrophy conserving scheme applied on the vorticity-stream function form. (d) Arakawa scheme with minimum artificial viscosity for controling numerical oscillations (diffusion constant $\kappa = 5.0 \times 10^{-7}$ m^2/s).

decrease when a non-oscillatory scheme is used. In order to see if this development can be explained with viscous turbulence theory (Lesieur, 1990), the time-development of kinetic energy, enstrophy and palinstrophy is also studied.

For the vorticity, the initial field is

$$\zeta(x, y, 0)=\begin{cases}\varepsilon \cos x-\delta \cosh^{-2}[(y-\pi/2)/\delta], \\ \quad y \leqslant \pi, \\ \varepsilon \cos x+\delta \cosh^{-2}[(3\pi/2-y)/\delta], \\ \quad y>\pi,\end{cases} \tag{20}$$

with $\varepsilon=0.05$ and $\delta=15/\pi$. This initial field is integrated in a doubly periodic domain of size $2\pi \times 2\pi$ to the final time $t=20.0$ with $\mathrm{CFL}_{\max}=0.5$, at the resolution 256^2, giving $\Delta x=\Delta y=\pi/128$ (see Fig. 7 of Hólm, 1995, for the time evolution of this initial field up to $t=10$).

Fig. 2 shows the vorticity at $t=8$ for the non-oscillatory scheme FPM4 applied to the momentum-pressure and the vorticity-stream function form, Figs. 2a–b, and the solutions from the Arakawa scheme without artificial viscosity and with the minimum artificial viscosity required to control the numerical oscillations ($\kappa=5.0 \times 10^{-7}\ \mathrm{m^2/s}$), Figs. 2c–d. Both non-oscillatory simulations, Figs. 2a–b, are smooth and almost indistinguishable, whereas the Arakawa reference scheme, Fig. 2c, has significant small scale oscillations, which are removed by applying artificial viscosity, Fig. 2d. The maximum value of the vorticity is 4.85 with FPM4/M, 4.78 with FPM4/V, 6.09 with AEE, and 4.92 with AEE + DF. The maximum amplitude of the numerical oscillations for AEE and for AEE + DF are ca. 1.5 and 0.25, respectively (see Section 3 for notations). It is possible to remove the oscillations of the Arakawa scheme almost completely, by doubling the artificial viscosity, but then the conservation properties will become unacceptable, at least compared to the high-order non-oscillatory schemes.

In Fig. 3, the time-development of the kinetic energy, the enstrophy and the palinstrophy are shown for the four simulations in Fig. 2, and for two extra simulations performed with the non-oscillatory scheme FPM2 applied to both forms of the equations. In all simulations, kinetic energy is conserved within 0.5%. For AEE and FPM4/V, there is a slight increase in kinetic energy, which

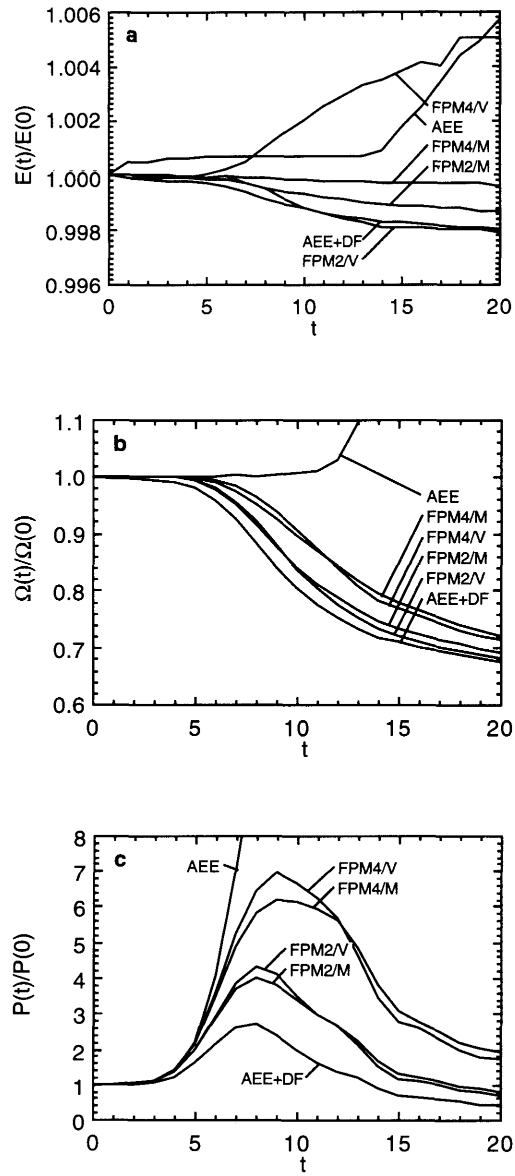

Fig. 3. Time-evolution for the shear-layer simulation up to $t=20$ (256^2 resolution, $\mathrm{CFL}_{\max}=0.5$). (a) Kinetic energy. (b) Enstrophy. (c) Palinstrophy. The values are normalized by their initial values: FPM2/M and FPM4/M are non-oscillatory schemes applied to the momentum-pressure form; FPM2/V and FPM4/V are applied to the vorticity-stream function form; AEE is the Arakawa scheme; AEE + DF is the Arakawa scheme with artificial viscosity (the diffusion constant $\kappa=5.0 \times 10^{-7}\ \mathrm{m^2/s}$ is the minimum necessary for controling numerical oscillations).

indicates that the second order-accurate time-stepping algorithm used in the present paper for the vorticity-stream function formulation is weakly unstable. The momentum-pressure versions FPM2/M and FPM4/M preserve the kinetic energy best. The enstrophy is dissipated, except for the Arakawa "energy and enstrophy conserving" scheme. Here, the enstrophy is first conserved, but it finally grows very large due to the ever increasing small scale oscillations. If artificial viscosity is added to the Arakawa scheme in order to remove the oscillations, then the enstrophy dissipation is slightly larger than for the non-oscillatory schemes. The explosive enstrophy increase in the simulation with the Arakawa scheme is surprising, until it is recalled that the Arakawa scheme is exactly energy and enstrophy conserving only for continuous time. When time is discretized, the exact conservation is generally lost (note, however, that Walsteijn, 1994, has developed time-stepping which in combination with the Arakawa energy or enstrophy conserving scheme gives exact conservation). The palinstrophy evolution is realistic in the non-oscillatory simulations, with an exponential build-up period up to $t \approx 8$, and a decrease during the later self similar decay stage, which is characteristic of freely decaying turbulence (Lesieur, 1990). Note that the enstrophy decay during the later stage of the evolution is also consistent with the theory.

The enstrophy spectrum at $t = 20$ is shown for some of the above simulations in Fig. 4. For homogeneous isotropic turbulence there should be

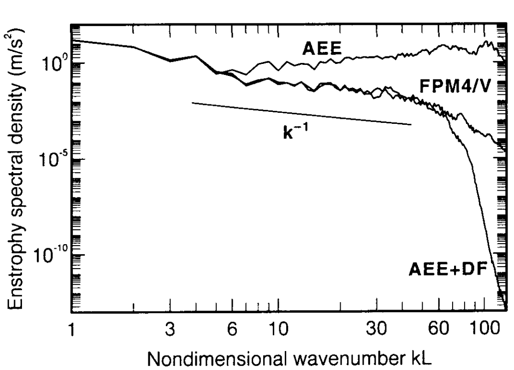

Fig. 4. Enstrophy spectra for the shear-layer simulation at $t = 20$ (256^2 resolution, $\mathrm{CFL}_{\max} = 0.5$) for three different schemes: FPM4/V, AEE and AEE + DF ($\kappa = 1.25 \times 10^{-7}$ m²/s).

an inertial range in the enstrophy spectrum with slope of -1 to -2 (corresponding to a slope of -3 to -4 in the kinetic energy spectrum). The non-oscillatory scheme, FPM4/V, has a realistic enstrophy spectrum with an inertial subrange slope -1.2. Above wavenumber 40–50, the amplitude falls of as k^{-5}. However, the structure of the spectrum is irregular due to the anisotropy of the flow field. When the Arakawa scheme is used, a build-up of enstrophy takes place in the smallest scales, since no enstrophy can leave the resolved scales, and the spectrum is totally unrealistic. When the scheme is supplemented with artificial viscosity, $\kappa = 1.25 \times 10^{-7}$ m²/s, the inertial subrange is similar to the non-oscillatory simulation, but the spectrum falls of much quicker, as k^{-30}, above wavenumber 70. In the spectrum for $\kappa = 5.0 \times 10^{-7}$ m²/s (not shown) this damping of short waves sets in already at wavenumber 50.

The effects of the non-oscillatory schemes and the Arakawa scheme with artificial viscosity are thus similar. The important differences are that there is larger diffusion and deformation of the spectrum when fourth order linear diffusion is used to obtain non-oscillatory results. An advantage of the non-oscillatory scheme is that no flow dependent tuning of the dissipation is needed. When a discontinuous shear layer is used as an initial condition ($\delta \to \infty$ in eq. (20)) and integrated to $t = 10$ (FPM4, $\mathrm{CFL}_{\max} = 0.5$, at the resolution 64^2), then the kinetic energy reduces to 96% and the enstrophy reduces to 23% of its initial value. In this case the Arakawa scheme gives 20% increase in kinetic energy and the enstrophy grows without control. Dissipation is needed to control the enstrophy, but its magnitude is larger this time. A decrease in $\mathrm{CFL}_{\max}$ from 0.5 to 0.1 damps the increase in enstrophy, but does not remove the oscillations.

In conclusion, high-order non-oscillatory schemes give automatic control of numerical oscillations. The enstrophy spectrum is realistic, but is however not as regular as in isotropic turbulence due to the anisotropy of the flow. The evolution of the flow is also consistent with the theory of incompressible viscous two-dimensional turbulence: there is an approximate kinetic energy conservation, and enstrophy is dissipated at the correct rate. However, when fourth order linear diffusion is used to obtain non-oscillatory results with the Arakawa scheme, the diffusion is larger and the high-wavenumber portion of the spectrum is deformed more than with a non-oscillatory scheme.

5.2. Homogeneous isotropic turbulence simulations

The shear layer test in the previous section gives enstrophy spectrum with a realistic slope, but the form of the spectrum is irregular due to the anisotropy of the flow. An isotropic turbulence simulation is needed in order to make the connection to theory more convincing. For this purpose an isotropic random initial vorticity field with a Gaussian distribution is constructed. The field is constructed by assigning each wave of the initial field a random amplitude, equally distributed in $[-1, 1]$, and then each amplitude is multiplied by a Gaussian distribution, so that the resulting initial field has the following wavenumber distribution (see also Fig. 6a)

$$\zeta(k, 0) = \sum_{k-1/2<|\boldsymbol{k}'|<k+1/2} \zeta(\boldsymbol{k}', 0) = \frac{k}{\sigma\sqrt{2\pi}} \exp[-(k-k_{\mathrm{m}})^2/(2\sigma^2)], \tag{21}$$

where the wavenumber magnitude is $k=|\boldsymbol{k}|=|(k_x, k_y)|$, the mean wavenumber is given by k_{m} and the standard deviation by σ. Only sine components are included, which means that there is a certain symmetry in the initial field (Brachet et al., 1988). In the tests the values used are $k_{\mathrm{m}}=6/L=6/(2\pi)\ \mathrm{m}^{-1}$ and $\sigma=2/L=2/(2\pi)\ \mathrm{m}^{-1}$. With these values, the initial field is well resolved with a 64^2 resolution. In the simulations, the resolutions are 64^2, 128^2, 256^2, and 512^2. Only the vorticity-stream function formulation is used in the simulations reported in this section.

Fig. 5 gives the time-development of the energy, enstrophy and palinstrophy (enstrophy dissipation). Freely decaying two-dimensional turbulence goes through two distinct stages. During the first stage, the palinstrophy grows exponentially until the viscosity becomes dominant, and thereafter the palinstrophy decreases proportional to t^{-3} (Lesieur, 1990). The evolution of the palinstrophy in the simulations is consistent with this picture, although it is not possible to see whether the decay is proportional to t^{-3} or for example t^{-2}. It is noteworthy, that there is a large difference between the two high-order non-oscillatory advection schemes in terms of kinetic energy conservation (Fig. 5a). The FPM4 scheme conserves as much energy at a 64^2 resolution as the FPM2 scheme at 256^2 resolution. Further, the palinstrophy attains higher amplitudes when FPM4 is used. The

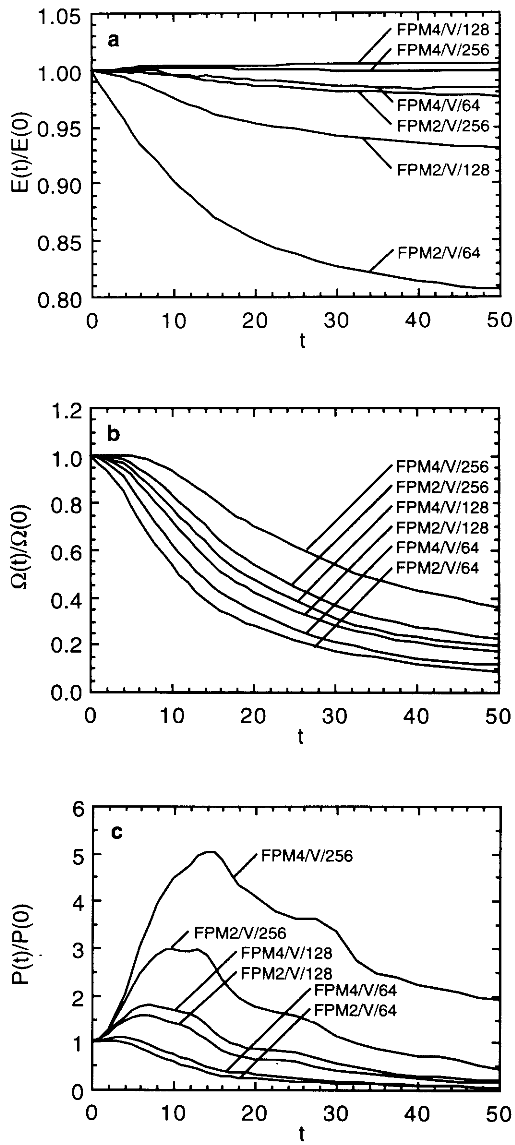

Fig. 5. Time-evolution for the freely decaying turbulence simulation up to $t=50$ (64^2, 128^2, and 256^2 resolution, $\mathrm{CFL}_{\max}=0.5$). (a) Kinetic energy. (b) Enstrophy. (c) Palinstrophy. FPM2/V/64 refers to a simulation with FPM2, vorticity-stream function formulation and 64^2 resolution, etc.

enstrophy dissipates for both schemes at a similar rate, where again FPM4 and higher resolution give less dissipation. Even if it is not possible to see whether the simulated enstrophy decays proportional to the theoretical value t^{-2}, it can be seen that the enstrophy dissipates at a lower rate than the palinstrophy, which is consistent with the theory.

In Fig. 6, the development of the enstrophy spectrum for the 256^2 FPM4 simulation is shown. From Fig. 5c it is known that the palinstrophy reaches a maximum at $t \approx 14$, whereafter it decays. Fig. 6a gives the evolution of the spectrum up to this time, and it is seen that this stage is characterized by a build-up of a spectrum with an inertial subrange. In Fig. 6b the subsequent evolution of the spectrum is displayed, and it is seen that the spectrum decays self-similarly, with an inertial subrange slope -1.2. This behaviour is consistent with the theoretical predictions for freely decaying two-dimensional viscous turbulence discussed above (Lesieur, 1990). Finally, Fig. 6c shows the palinstrophy (enstrophy dissipation) spectrum during the decay period of the simulation. Most of the amplitude is concentrated between wavenumbers 30 and 50, and only waves longer than this can be accurately represented in the present simulation. It is also seen that the implicit viscosity of the non-oscillatory scheme works as a filter which in the present simulation causes the spectrum to fall off approximately as k^{-5} above wavenumber 40–50.

In order to get some measure of how accurate the simulation is, the 256^2 FPM4 enstrophy spectrum is compared with a 512^2 FPM4 solution at $t = 14$ and $t = 18$. These times are chosen from the consideration that the simulations are essentially inviscid and accurate for the resolved scales during the build-up period of the flow, which at 256^2 resolution ends at $t = 14$ for FPM4. Therefore the simulations should be quite accurate at this time at both resolutions, which is indeed seen in Fig. 7a, where the two (unfiltered) spectra coincide for wavenumbers less than 30, and have a similar detailed form above this wavenumber, although the slope is different there. At $t = 18$ the coarser resolution simulation has entered the decaying stage, whereas the finer resolution simulation has just reached the peak in the palinstrophy evolution (not shown) and is therefore still quite accurate. There are now visible differences in the spectra,

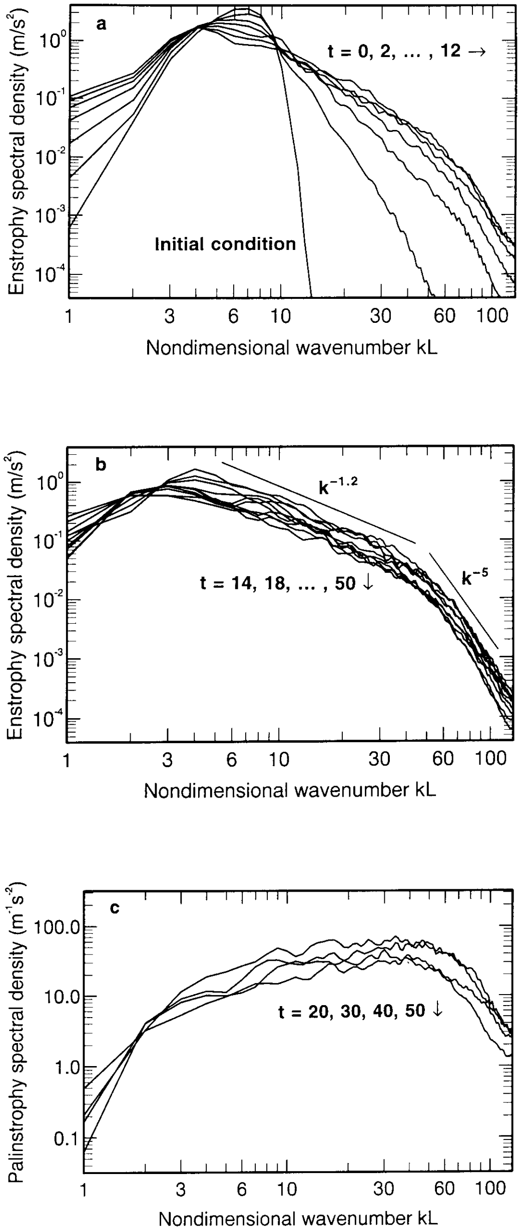

Fig. 6. Spectra for the freely decaying turbulence simulation up to $t = 50$ (256^2 resolution, $CFL_{max} = 0.5$) for FPM4/V. (a) Enstrophy spectra during the build-up phase of the flow, $t = 0, 2, ..., 12$. (b) Enstrophy spectra during the self-similarly decaying phase of the flow, $t = 14, 18, ..., 50$. (c) Palinstrophy (enstrophy dissipation) spectra during the self-similarly decaying phase of the flow, $t = 20, 30, 40, 50$.

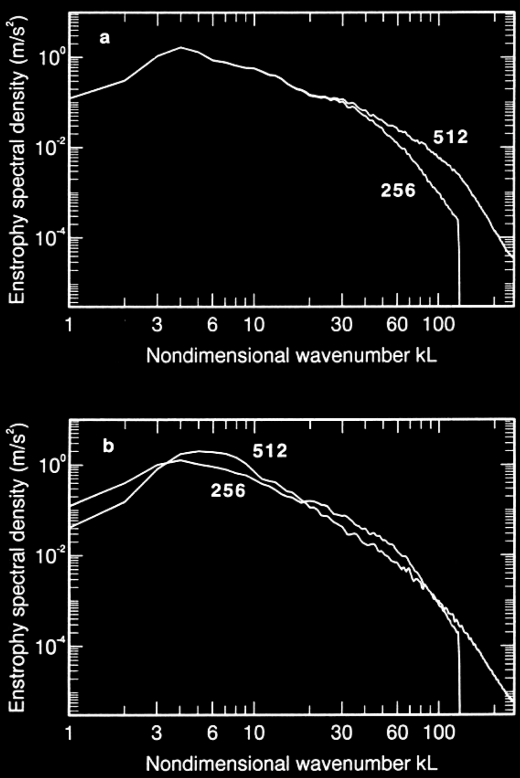

Fig. 7. Comparison between enstrophy spectra for the freely decaying turbulence simulation at 256^2 and 512^2 resolution (FPM4/V, $\mathrm{CFL_{max}} = 0.5$). (a) $t = 14$ (time of maximum palinstrophy in the 256^2 simulation). (b) $t = 18$ (time of maximum palinstrophy in the 512^2 simulation).

Fig. 7b. The shear layers in the high-resolution simulation have just reached the minimum thickness which can be supported by the non-oscillatory advection scheme, and the Reynolds number, eq. (15), has decreased from $R_l \approx 40000$ at $t = 0$, to $R_l \approx 25$ at $t = 18$. In the low-resolution simulation, the solution has passed the point when the shear layers could be supported by the non-oscillatory scheme, and the implicit viscosity has already influenced the simulation considerably ($R_l \approx 5000$ at $t = 0$, has decreased to $R_l \approx 19$ at $t = 18$). But in physical space, the two fields are still quite similar, Fig. 8a–b, and the lower resolution simulation looks like a smoothed, or averaged, version of the higher resolution simulation, with the different flow features in the right place. This is the essence of a finite-volume integration technique, which makes it useful for simulating flows with unresolved scales.

The difference between the two spectra in Fig. 7a is no coincidence, and can be understood from both mathematical and physical considerations. If a spectrum is truncated at a given wavenumber, and then transformed back to physical space, there will always appear oscillations which were not present in the original, untruncated field. This is simply Gibbs' phenomenon. In order to avoid oscillations in the truncated field, it is necessary to multiply the truncated spectral coefficients with a "window" function, which decreases the amplitude of the shortest waves, while the long waves are unaffected. In signal processing, so called smooth filters are used to achieve this effect, e.g., the Butterworth filter (see Hamming, 1989). These filters have the side effect of chopping peaks and filling in valleys of the original field. But with a high-order smooth filter it is possible to minimize

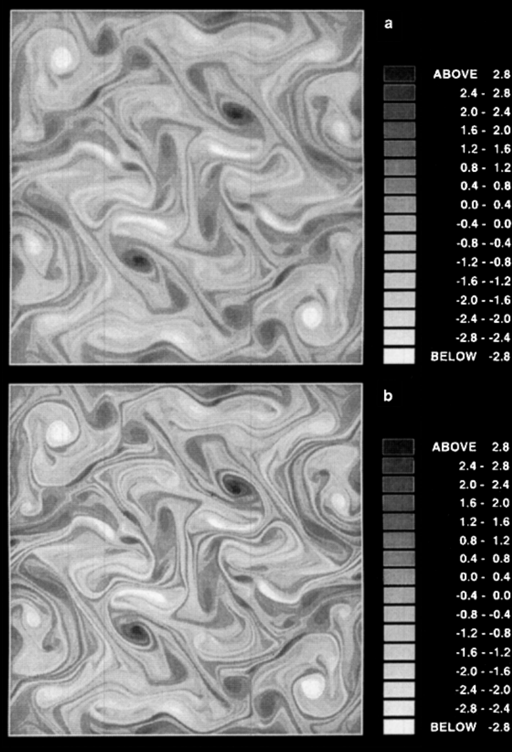

Fig. 8. Vorticity field for the freely decaying turbulence simulation at $t = 18$. (FPM4/V, $\mathrm{CFL_{max}} = 0.5$): (a) 256^2 resolution, and (b) 512^2 resolution.

this effect. The analogy to Fig. 7a is obvious. The high resolution simulation can be assumed to be very close to the continuous solution for wavenumbers less than 128. The spectrum of the low resolution simulation then looks as a truncated version of the full spectrum which has been multiplied by a smooth window function. The appearance of the truncated physical solution is also consistent with this picture: no oscillations, but the low resolution solution, Fig. 8a, looks like a smoothed version of the high resolution field, Fig. 8b.

Another explanation of the damping of high wavenumbers is obtained from considering the enstrophy flux between different wavenumbers. Due to nonlinear interactions, every wave will interact with larger as well as with shorter waves. This interaction gives rise to a net enstrophy flux across the wavenumber range. When the wavenumber range is truncated, the non-oscillatory advection scheme can be interpreted as a one-way filter, which allows a flow of enstrophy from the resolved to the unresolved wavenumber range, but which does not receive any feedback from unresolved wavenumbers. This process will in the long run create an unnatural damping of the resolved waves, as compared with the full spectrum of the flow. In particular, the flow from resolved to unresolved scales is obvious during the build-up period of the inertial subrange (as in Fig. 6a).

Further understanding of how the implicit viscosity of the non-oscillatory schemes works can be obtained by considering the evolution of the system described by either eqs. (1–3) or eqs. (4–7), see also Fig. 8. The vorticity is here concentrated in shear layers, which shrink and elongate with time. As the shear layer shrinks, viscosity becomes important and smoothes the vorticity distribution. Eventually the effect of viscosity hinders the shear layer from shrinking further. When the equations are used without viscous terms, as in the present case, the minimum width of the shear layer is determined by the resolution, i.e., by the gridcell size h or a maximum wavenumber k_N. When a non-oscillatory advection scheme is used, the minimum size of the shear layer is larger than one gridcell. High-order non-oscillatory advection schemes can maintain large gradients over one to three gridcells, whereas low-order non-oscillatory schemes, like the upstream scheme, may smear the shear layer over several gridcells. Near large gradients, a non-oscillatory advection scheme automatically damps the advected field just enough in order not to create unphysical over- or undershoots. The effect is that the maximum resolvable wavenumber is smaller than the theoretically resolvable.

Finally, the different aspects of an ideal model, mentioned in the introduction, can now be reconsidered. On one hand, an ideal model should have a perfect spectrum in the resolvable wavenumber range, and on the other, an ideal model should be conserving and free of numerical oscillations, i.e., non-oscillatory. But due to Gibbs' phenomenon, it is impossible to have a truncated model which fulfils these two requirements simultaneously. The best one can hope for is a good balance between these two aspects. If the small scale motions are important for the model, e.g., for obtaining realistic statistics for the atmosphere in a general circulation model, then the perfect spectrum aspect should be emphasized. If it is important that small scale oscillations do not occur, e.g., in a weather forecast model, where the interaction of the small scale oscillations with cloud physics and other processes could destabilize the model integration, then the non-oscillatory aspect should be stressed.

In summary, the isotropic turbulence test shows convincingly that the conservative and spectral properties of the high-order non-oscillatory schemes are very good. The balance between obtaining a non-oscillatory physical solution and a realistic spectrum is about as good as can be hoped for from theory, and much better than what can be obtained with linear fourth order diffusion applied to Arakawa's energy and enstrophy conserving scheme. The simulations essentially conserve the kinetic energy of the large scales, and the enstrophy is dissipated at the correct rate predicted by turbulence theory.

6. Conclusions

In the present paper the high-order, non-oscillatory advection schemes of Hólm (1995) are applied to two important forms of the equations of non-elastic flow: the momentum-pressure form and the vorticity-stream function form. When fully second-order accurate time-integration techniques are used, including a second order accurate integration of source terms, both formulations essentially conserve kinetic energy and dissipate enstrophy. High-order non-oscillatory advection schemes automatically control the numerical instabilities, which originally motivated the use of artificial viscosity in atmospheric models, and thus no artificial viscosity is needed in addition to a non-oscillatory advection scheme (if other model processes are properly formulated).

It is argued in the paper, that simulations performed with non-oscillatory advection schemes will in effect behave as viscous flows in the interior of the fluid, even if the governing equations without viscosity are used, due to the built-in implicit viscosity of non-oscillatory schemes. This has several consequences.

First, the theory of viscous, incompressible, two-dimensional turbulence can be used for controlling the accuracy of the simulations, instead of analytic solutions, which only exist for very simple flows. With this approach, the development of energy, enstrophy, and the enstrophy dissipation (palinstrophy) are shown to be consistent with the theory of viscous turbulence in the high-order non-oscillatory simulations. In particular, the palinstrophy at first grows exponentially, until it levels of and then decays, whereas the enstrophy decays all the time, but at a lower rate than the palinstrophy.

Second, the viscous turbulence theory can be used to define an effective viscosity (which is flow dependent) for the non-oscillatory schemes, even if there are no viscous terms in the governing flow equations. With this effective viscosity, several characteristics of the flow, like Reynolds numbers etc., can be calculated. Further, the magnitude of the effective viscosity can be used to detect potential problems when the non-oscillatory advection schemes are incorporated in models with parametrizations of subgrid scale processes. The effective viscosity should be small enough to affect the model variables negligibly compared with the contribution from the parametrization of subgrid scale processes like vertical diffusion processes, gravity wave propagation, boundary layer processes and surface energy exchanges. The high-order non-oscillatory scheme with fourth degree polynomials applied to the vorticity-stream function formulation is most promising from this point of view, since it has two-orders of magnitude less effective viscosity for long waves than other tested schemes.

Third, the turbulence theory is useful for predicting the spectral appearance of the simulations. The enstrophy spectrum of freely decaying, two-dimensional, viscous turbulence should have an inertial subrange with a slope between -1 and -2, depending on how much large scale eddies are present. In simulations both of a developing shear layer and of isotropic turbulence, an inertial subrange with a slope of -1.2 is observed. The time-development of the spectrum closely follows theory. First the spectrum goes through a stage when the inertial subrange builds up. During this stage the enstrophy dissipation also grows exponentially. Then follows a stage of self similar decay, during which the enstrophy dissipation also decays.

A problem with the enstrophy spectrum of the non-oscillatory simulation is the steep decay, $\sim k^{-5}$, of the upper half of the wavenumber range. In order to understand the reason for this damping of the shorter waves, the origin and the effect of the implicit diffusion in non-oscillatory advection schemes is analysed. When a spectrum is truncated at a given wavenumber, and the truncated spectrum is transformed back to physical space, then oscillations will appear which were not present in the original field, due to Gibbs' phenomenon. By making an analogy with the "smooth filters" used in signal processing, it is shown that the truncated spectrum must be modified, by decreasing the amplitude of the shortest waves, for the physical truncated solution to be non-oscillatory. Thus it is impossible to have a perfect spectrum and a non-oscillatory physical field for a truncated model. A balance has to be found between these two aspects from case to case. If the non-oscillatory aspect is more important, then the high-order, non-oscillatory schemes give better conservation properties and a more realistic spectrum than the reference Arakawa scheme with fourth order linear artificial viscosity. The non-oscillatory aspect is essential when the advection process is coupled to other physical processes and parametrizations in atmospheric models.

A general conclusion of the studies performed in this paper is that high-order non-oscillatory advection schemes have the properties required for the simulations of large-scale atmospheric flows. The only potential drawback of high-order, non-oscillatory advection schemes is that they are generally computationally more expensive than simple, centred, finite difference schemes. This brings one back to the problem that a balance has to be found between the accuracy of the atmospheric simulation, and the time required to complete the calculations. Obviously high-order, non-oscillatory advection schemes are accurate for complex atmospheric flows. But a further study has to be made of the efficiency of this approach. Simulations of elastic flows, in particular the simulation of the shallow water equations on a sphere (Williamson et al., 1992), are required for a convincing answer to the question whether the high-order, non-oscillatory advection schemes are competitive in large-scale atmospheric models.

7. Acknowledgements

I especially thank Dr. Erland Källén, who suggested this study, read through several versions of the manuscript, and contributed with many ideas which found their way into the work. I also thank Dr. Philip Rasch and Dr. Gerhard Erbes for reading the manuscript and making important comments.

REFERENCES

Arakawa, A. 1966. Computational design for long-term numerical integration of the equations of fluid motion. Two-dimensional incompressible flow. Part I. *J. Comput. Phys.* **1**, 119–143.

Arakawa, A. and Hsu, Y.-J. G. 1990. Energy conserving and potential enstrophy dissipating schemes for the shallow water equations. *Mon. Wea. Rev.* **118**, 1960–1969.

Basdevant, C., Lesieur, M. and Sadourny, R. 1978. Subgrid-scale modeling of enstrophy transfer in two-dimensional turbulence. *J. Atmos. Sci.* **35**, 1028–1042.

Bell, J. B., Colella, P. and Glaz, H. M. 1989. A second-order projection method for the incompressible Navier-Stokes equations. *J. Comput. Phys.* **85**, 257–283.

Brachet, M. E., Meneguzzi, M., Politano, H. and Sulem, P. L. 1988. The dynamics of freely decaying two-dimensional turbulence. *J. Fluid Mech.* **194**, 333–349.

E, W. and Shu, C.-W. 1994. A numerical resolution study of high order essentially non-oscillatory schemes applied to incompressible flow. *J. Comput. Phys.* **110**, 39–46.

Gage, K. S. and Nastrom, G. D. 1986. Theoretical interpretation of atmospheric wavenumber spectra of wind and temperature observed by commercial aircraft during GASP. *J. Atmos. Sci.* **43**, 729–740.

Grinstein, F. F. and Guirguis, R. H. 1992. Effective viscosity in the simulation of spatially evolving shear flows with monotonic FCT models. *J. Comput. Phys.* **101**, 165–175.

Gupta, M. M. 1991. High accuracy solutions of incompressible Navier-Stokes equations. *J. Comput. Phys.* **93**, 343–359.

Hamming, R. W. 1989. *Digital filters*, 3rd edition. Prentice-Hall International, Inc., Englewood Cliffs, 284 pp.

Herring, J. R., Orszag, S. A., Kraichnan, R. H. and Fox, D. G. 1974. Decay of two-dimensional homogeneous turbulence. *J. Fluid Mech.* **66**, 417–444.

Hirsch, C. 1990. *Numerical computation of internal and external flows, vol. 2. Computational methods for inviscid and viscous flows.* John Wiley & Sons Ltd., 691 pp.

Hólm, E. V. 1995. A fully two-dimensional, non-oscillatory advection scheme for momentum and scalar transport equations. *Mon. Wea. Rev.* **123**, 536–552.

Lesieur, M. 1990. *Turbulence in fluids. Stochastic and numerical modelling*, 2nd edition. Kluwer Academic Publishers, 412 pp.

Monin, A. S. and Ozmidov, R. V. 1985. *Turbulence in the ocean.* D. Reidel Publishing Company, 247 pp.

Pouquet, A., Lesieur, M., André, J. C. and Basdevant, C. 1975. Evolution of high Reynolds number two-dimensional turbulence. *J. Fluid Mech.* **72**, 305–319.

Sadourny, R. and Basdevant, C. 1985. Parametrization of subgrid scale barotropic and baroclinic eddies in quasi-geostrophic models: Anticipated Potential Vorticity Method. *J. Atmos. Sci.* **42**, 1353–1363.

Smolarkiewicz, P. K. and Margolin, L. G. 1993. On forward-in-time differencing for fluids: Extension to a curvilinear framework. *Mon. Wea. Rev.* **121**, 1847–1859.

Smagorinsky, J. 1993. Some historical remarks on the use of nonlinear viscosities. *Large eddy simulation of complex engineering and geophysical flows.* B. Galperin and S. A. Orzag, eds. Cambridge University Press, 3–36.

Taylor, G. I. 1960. The decay of eddies in a fluid. *The scientific papers of Sir Geoffrey Ingram Taylor*, vol. II, G. K. Batchelor, ed. Cambridge University Press, pp. 190–192.

Walsteijn, F. H. 1994. Robust numerical methods for 2D turbulence. *J. Comput. Phys.* **114**, 129–145.

Williamson, D. L., Drake, J. B., Hack, J. J., Jacob, R. and Swarztrauber, P. N. 1992. A standard test for numerical approximations to the shallow water equations in spherical geometry. *J. Comput. Phys.* **102**, 211–224.